HOKKAIDO UNIVERSITY

Title	Immunolocalization of DMP1 and sclerostin in the epiphyseal trabecule and diaphyseal cortical bone of osteoprotegerin deficient mice
Author(s)	Masuki, H.; Li, Minqi; Hasegawa, T.; Suzuki, R.; Guo, Y.; Liu, Z.; Oda, K.; Yamamoto, T.; Kawanami, M.; Amizuka, N.
Citation	Biomedical Research, 31(5), 307-318 https://doi.org/10.2220/biomedres.31.307
Issue Date	2010-11-10
Doc URL	http://hdl.handle.net/2115/72271
Type	article
File Information	A2_31_307.pdf

Instructions for use

Hokkaido University Collection of Scholarly and Academic Papers : HUSCAP

Biomedical Research **31** (5) 307-318, 2010

Immunolocalization of DMP1 and sclerostin in the epiphyseal trabecule and diaphyseal cortical bone of osteoprotegerin deficient mice

Hideo MASUKI[1, 2], Minqi LI[1], Tomoka HASEGAWA[1], Reiko SUZUKI[1], Guo YING[1, 2], Liu ZHUSHENG[1], Kimimitsu ODA[3], Tsuneyuki YAMAMOTO[1], Masamitsu KAWANAMI[2] and Norio AMIZUKA[1]

Departments of [1] Developmental Biology of Hard Tissue and [2] Periodontology and Endodontology, Graduate School of Dental Medicine, Hokkaido University, Sapporo 060-8586, and [3] Division of Biochemistry, Niigata University Graduate School of Medical and Dental Sciences, Niigata 951-8514, Japan

(Received 30 July 2010; and accepted 20 August 2010)

ABSTRACT

In order to define the osteocytic function in accelerated bone remodeling, we examined the distribution of the osteocytic lacunar-canalicular system (OLCS) and osteocyte-secreting molecules—dentin matrix protein (DMP) 1 and sclerostin—in the epiphyses and cortical bones of osteoprotegerin deficient ($OPG^{-/-}$) mice. Silver impregnation visualized a well-arranged OLCS in the wild-type epiphyses and cortical bone, whereas $OPG^{-/-}$ mice had an irregular OLCS in the epiphyses, but well-arranged canaliculi in the cortical bone. DMP1-positive osteocytes were evenly distributed throughout the wild-type epiphyses and cortical bone, as well as the $OPG^{-/-}$ cortical bone. However, $OPG^{-/-}$ epiphyses revealed weak DMP1-immunoreactivity. Thus, osteocytes appear to synthesize more DMP1 as the OLCS becomes regular. In contrast, sclerostin-immunoreactivity was significantly diminished in the $OPG^{-/-}$ epiphyses and cortical bone. In $OPG^{-/-}$ epiphyses and cortical bone, triple staining demonstrated few sclerostin-positive osteocytes in the periphery of a thick cell layer of alkaline phosphatase-positive osteoblasts and many tartrate resistant acid phosphatase-positive osteoclasts. Summarizing, the regular distribution of OLCS may affect DMP1 synthesis, while the cellular activities of osteoclasts and osteoblasts rather than the regularity of OLCS may ultimately influence sclerostin synthesis.

Osteocytes are the most numerous cells in bone, being localized within their lacunae. The osteocytes are connected each other by means of their cytoplasmic processes interconnected through gap junctions (9, 23), which pass through narrow passage ways referred to as osteocytic canaliculi. Therefore, osteocytes build up functional syncytia, *i.e.*, the osteocytic lacunar-canalicular system (OLCS) (1, 7, 15). To date, osteocytes and their canaliculi have been shown to sense the direction and strength of mechanical stress in bone and then, affect the communication among osteocytes and between osteocytes and osteoblasts (7, 14, 35). They may also regulate bone remodeling (16, 22, 27) and mineral metabolism (4, 10, 27). Osteocytes might control trafficking of minerals such as calcium and phosphate through their canaliculi, and might regulate osteoclastic and osteoblastic activities on the bone surface. These putative functions imply that OLCS feature a finely tuned arrangement, which may be altered by physical or chemical imbalances.

Our previous work demonstrated that physiological bone remodeling would reconstruct the arrangement of OLCS more regularly; especially, the speed of bone deposition during remodeling would influence the regularity of OLCS (13, 31). The regularity of OLCS appears to be different in each region of

Address correspondence to: Dr. Hideo Masuki, Department of Periodontology and Endodontology, Graduate School of Dental Medicine, Hokkaido University, Kita 13, Nishi 7, Kita-Ku, Sapporo, Hokkaido 060-8586, Japan
Tel & Fax: +81-11-706-4226
E-mail: i-elm@aria.ocn.ne.jp

long bones, probably due to the different speed of bone remodeling. For example, epiphyses and cortical bone are independent of longitudinal bone growth driven by endochondral bone formation, and therefore, its bone remodeling appears to be slower than that seen in the metaphyses. The regularly-arranged OLCS accomplished by physiological bone remodeling in the epiphyses and cortical bone seems effective for their function—sensing mechanical stress, regulating bone remodeling and transporting minerals and chemicals (13, 31).

The synthesis of osteocyte-derived molecules may reflect the biological roles of OLCS, and therefore, investigation of their synthesis and localization would provide clues to understand osteocytic function. Dentin matrix protein (DMP) 1 was originally identified in rat incisor's pulp cDNA library (12). Later, DMP1 was shown to be a bone matrix protein expressed in osteocytes, and has been assumed to play a role in bone mineral homeostasis, due to its high calcium ion-binding capacity (29). As shown in a recent report that a lack of DMP1 gave rise to rickets or osteomalacia in mice (10), a possible role of osteocytes mediating DMP1 appears to be local regulation of mineralization.

Sclerostin is a glycoprotein which is a product of the *SOST* gene, and secreted by osteocytes (37). It was reported to bind the LRP5/6 receptor, thereby antagonizing Wnt signaling and increasing β-catenin degradation (18, 34). Sclerostin has been highlighted as a negative regulator of osteoblastic bone formation (22, 24, 32, 37), and is also regarded as an important mediator of mechanical loading in bone (20). Recently, treatment with the sclerostin antibody in a rat model of postmenopausal osteoporosis led to an increase in bone formation, bone mass and bone strength (19). Taken together, osteocytes are not merely resting cells embedded in bone, but appear to actively regulate bone metabolism by secreting sclerostin.

Physiological bone remodeling, the coupled bone resorption and formation which replace old bone with new one, seems necessary for building up the geometrical regularity of OLCS, as described (13, 31). Stimulated osteoclastogenesis and subsequent bone remodeling may provoke a disorganized OLCS. Osteoclastogenesis is chiefly controlled by the interaction between the receptor activator of the nuclear factor κB (RANK) and RANK ligand (RANKL). RANK is a member of the membrane-associated tumor necrosis factor receptor family located on cell membranes of osteoclasts and their precursors (17, 38), while RANKL is present on the cell membrane of osteoblast lineages (17, 30, 38). Cell-to-cell contact between osteoblastic cells and osteoclast precursors brings RANK into binding with RANKL, initiating osteoclastogenesis (2, 26, 28). Osteoprotegerin (OPG) acts as a decoy receptor for RANKL, preventing its association with RANK and inhibiting osteoclastogenesis (25). Therefore, mice homozygous for targeted disruption of the OPG gene reveal stimulated osteoclastogenesis and consequent bone resorption, and thereby, they are a valid model for extremely-stimulated bone remodeling (3, 36).

In this study, we aimed to elucidate the osteocytic function underlying the stimulated bone remodeling. Therefore, we employed the epiphyses and diaphyseal cortical bone from the $OPG^{-/-}$ mice, in which we could exclude the effects of individual bone growth, and histochemically examined the geometrical regularity of OLCS and the synthesis of osteocyte-derived molecules, *i.e.,* DMP1 and sclerostin.

MATERIALS AND METHODS

Tissue preparation. All animal procedures were performed on seventeen week-old male wild-type and $OPG^{-/-}$ mice (n = 6, for each) obtained as previously described (3), in accordance with guidelines for animal experimentation set by Hokkaido University. All mice were anesthetized with an intraperitoneal injection of chloral hydrate and perfused through the left ventricle with 4% paraformaldehyde diluted in 0.1 M phosphate buffer (pH 7.4). Femora were dissected free of soft tissue and immersed in the same fixative for an additional 12 h at 4°C. After decalcification with 5% EDTA-2Na solution for 2 weeks at 4°C, the specimens were dehydrated through a graded series of ethanol prior to being embedded in paraffin.

Histochemistry for tartrate resistant acid phosphatase (TRAP), alkaline phosphatase (ALP), sclerostin and DMP1. For detection of TRAP activity, the histological sections were incubated with a mixture of 2.5 mg of naphthol AS-BI phosphate (Sigma, St. Louis, MO), 18 mg of red violet LB salt (Sigma) and 100 mM L (+) tartaric acid (0.76 g; Nacalai Tesque, Kyoto, Japan) diluted in 30 mL of 0.1 M sodium acetate buffer (pH 5.0) for 15 min at 37°C.

For immunolocalization of ALP and sclerostin, deparaffinized sections were treated with 0.1% hydrogen peroxide for 15 min, to inhibit endogenous peroxidase, and pre-incubated with 1% bovine serum albumin in phosphate buffered saline (BSA-PBS) for 30 min at room temperature. Rabbit antiserum

against tissue nonspecific ALP (21) was applied to the sections at a dilution of 1 : 300 overnight at 4°C. Sections were then incubated with horseradish peroxidase (HRP)-conjugated goat anti-rabbit IgG (DakoCytomation, Glostrup Denmark). For sclerostin detection, the sections were incubated with goat anti-sclerostin (R&D System Inc., Minneapolis, MN) at a dilution of 1 : 100, and subsequently incubated with HRP-conjugated anti-goat IgG (American Qualex, San Clemente, CA) at 1 : 100 at room temperature. Regarding immunodetection of DMP1, the deparaffinized sections were treated with 1 μg/mL trypsin (Wako Pure Chemical Industries Ltd., Osaka, Japan) for 30 min. After pre-incubation with 1% BSA-PBS for 30 min at room temperature, sections were incubated with rabbit antibody against DMP1 (Takara Bio Inc., Otsu, Japan) at a dilution 1 : 500 overnight at 4°C. Incubation with HRP-conjugated goat anti-rabbit IgG (DakoCytomation) was undertaken, and then, rinsed with PBS. Immune complexes were visualized using 3,3'-diaminobenzidine tetrahydrochloride (DAB, Dojindo Laboratories, Kumamoto, Japan).

For triple staining with sclerostin, ALP and TRAP, we at first performed sclerostin immunohistochemistry visualizing using DAB, and then, ALP detection by employing secondary antibody conjugated with ALP (Seikagaku Biobusiness Co. Tokyo, Japan). For enzyme histochemistry for ALP, the sections with the immune complex were incubated in an aqueous mixture of 2.5 mg of naphthol AS-BI phosphate (Sigma) and 18 mg of fast blue RR salt (Sigma) diluted in 30 mL of 0.1 M Tris-HCl buffer (pH 8.5) for 30 min at 37°C. Double stained sections carrying sclerostin and ALP colorized in brown and blue was finally subjected to TRAP detection as described above. All the sections were counterstained faintly with methyl green, and were observed under a Nikon Eclipse E800 microscope (Nikon Instruments Inc., Tokyo, Japan). Light microscopy images were acquired with a digital camera (Nikon DX-M1200C, Nikon, Japan).

Silver impregnation. We performed silver impregnation based on a modification of Bodian's protargol-S procedure (5, 6, 31). In brief, the dewaxed sections were soaked in a 1% Protargol-S solution diluted in borax-boric acid (pH 7.4) for 12–48 h at 37°C. After rinsing with distilled water, the reaction was enhanced by an aqueous solution containing 0.2% hydroquinone, 0.2% citric acid and 0.7% nitric silver. After additional rinsing, the sections were reacted for 5 min with a solution of 2.5 % anhydrous sodium sulfite, 0.5% potassium bromide and 0.5% amidol diaminophenol dihydrochloride. They were then treated with 1% gold chloride, and subsequently treated by 2% oxalic acid amidol until black staining of the osteocytic canaliculi could be visualized. After rinsing with distilled water, sections were fixed in 5% sodium thiosulfate.

Quantification of DMP1-positive or sclerostin-positive osteocytes, as well as ALP-positive or TRAP-positive areas. The total number of osteocytes and the number of DMP1-positive or sclerostin-positive osteocytes were counted in trabecular bones in the anterior region of the femoral epiphyses, or in a square (200 μm) encompassed by periosteal and endosteal surfaces in cortical bone, with the aid of ImagePro Plus 6.2 software (Media Cybernetics, Silver Spring, MD), as previously reported (11, 31). The percentage of the DMP1-positive or sclerostin-positive osteocytes was statistically analyzed between the wild-type and OPG$^{-/-}$ specimens (n = 6 per group). Regarding the quantification of ALP-positive or TRAP-positive areas, triple stained images of sclerostin, ALP and TRAP in the corresponding areas of the epiphyses and the diaphyseal cortical bones were obtained from wild-type and OPG$^{-/-}$ samples, and calculated as reported previously (11). Statistical analysis was performed using Microsoft Excel 2003 (Microsoft Corporation, Redmond, WA), and all values are presented as means ± standard deviation. Differences among groups were assessed by the paired Student's *t*-test, and considered statistically significant when $P < 0.05$.

RESULTS

Altered histology and distribution of OLCS in femoral epiphyses and cortical bones of OPG deficient mice

The histological sections from the femora of seventeen week-old adult OPG$^{-/-}$ mice exhibited an enclosure of the growth plate, resulting in fragmented islets of cartilage remnants (Figs. 1A, B). The amount and size of trabecular bone had decreased in the whole epiphysises of OPG$^{-/-}$ mice, while those in the anterior region of the epiphyses were not evidently different between the wild-type and OPG$^{-/-}$ mice (Figs. 1C, D). Although OPG$^{-/-}$ cortical bones were slightly porous due to infiltration of a soft tissue, the wild-type counterparts showed a compact profile (Figs. 1E, F).

Silver impregnation revealed well-arranged OLCS in the wild-type epiphyses, in which osteocytes

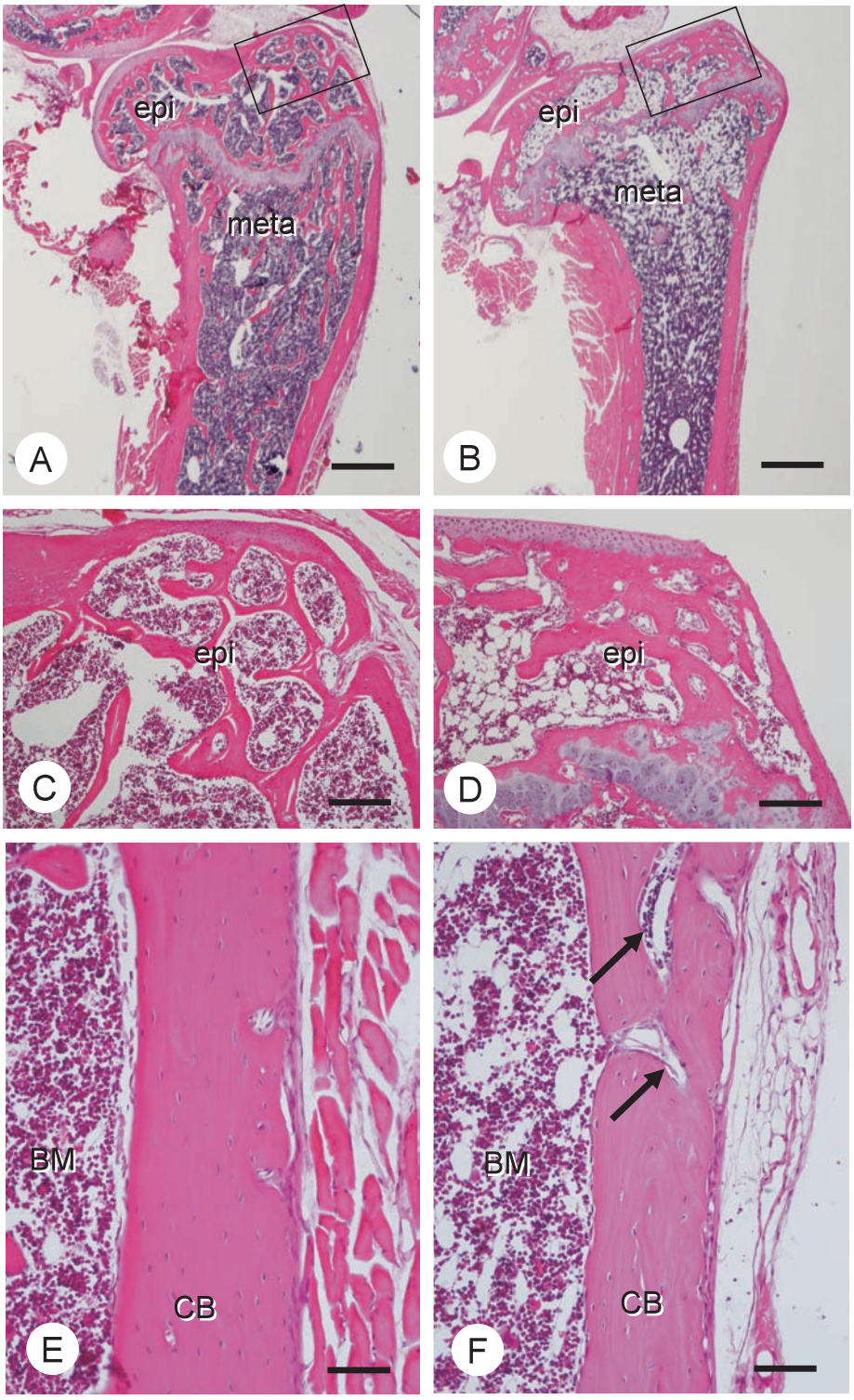

Fig. 1 Histological sections from the femora of wild-type mice (A, C, E) and OPG$^{-/-}$ mice (B, D, F). The epiphyses (epi) and metaphyses (meta) of the OPG$^{-/-}$ mice (B) showed fewer numbers of trabecules compared with the wild-type mice (A), and the OPG$^{-/-}$ femur exhibited an enclosure of the epiphyseal growth plate, resulting in fragmented islets of cartilage remnants (B). However, the anterior regions (indicating by squares in A and B) of the wild-type (C) and OPG$^{-/-}$ (D) epiphyses were not evidently different, showing similar numbers of trabecules. OPG$^{-/-}$ cortical bones (CB) were slightly porous permitting an infiltration of soft tissue (arrows, F), while the wild-type counterparts showed a compact profile (E). BM: bone marrow, Bars: 800 μm (A and B), 200 μm (C and D), and 100 μm (E and F)

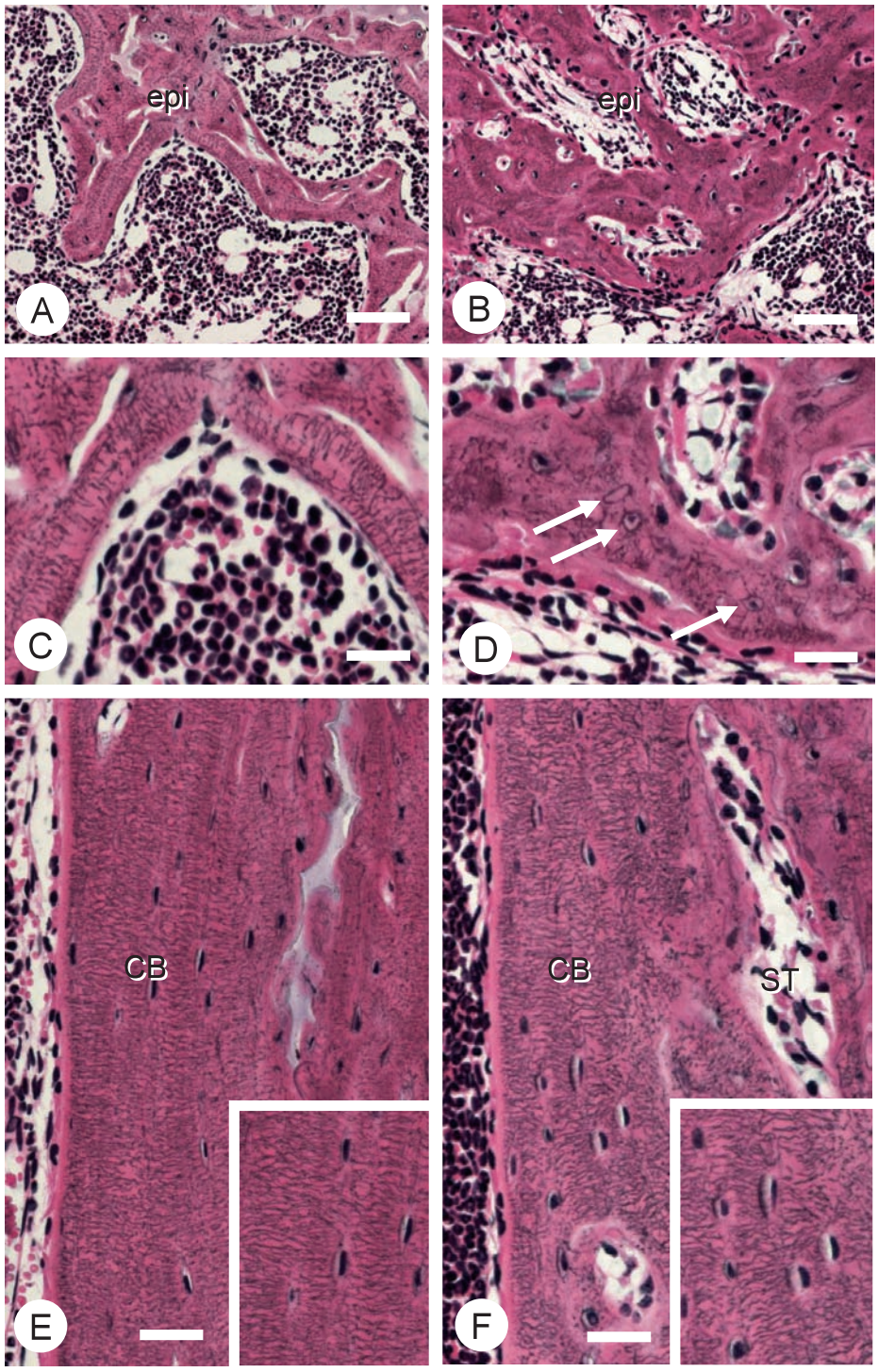

Fig. 2 Silver impregnation in the epiphyses of the wild-type (A, C, E) and OPG$^{-/-}$ (B, D, F) mice. Panels A (wild-type) and B (OPG$^{-/-}$) show lower magnified images of epiphyseal trabeculae. At higher magnification, the wild-type epiphyses (epi) revealed well-arranged OLCS, in which osteocytes extended their cytoplasmic processes in a well-arranged manner (C). In OPG$^{-/-}$ epiphyses, however, osteocytes were randomly-embedded extending their cytoplasmic processes in all directions, therefore, forming irregular distribution of OLCS (D). Note empty lacunae and lacunae with pyknotic osteocytes (arrows). The cortical bone (CB) of the wild-type mice (E) featured regularly-arranged OLCS (See an inset), in which the longitudinal axis of osteocytes was parallel to the bone surface, and the osteocytes extended their cytoplasmic processes perpendicular to the bone surface. The OPG$^{-/-}$ cortical bone also showed a well-aligned OLCS (an inset, F). However, the periphery of invading soft tissue (ST) revealed irregular distribution of osteocytes. Bars: 70 μm (A and B), 30 μm (C and D), and 40 μm (E and F)

extended their cytoplasmic processes in a well-arranged manner (Figs. 2A, C). In $OPG^{-/-}$ epiphyses, randomly-embedded osteocytes extended cytoplasmic processes in all directions (Figs. 2B, D). Several empty lacunae and lacunae with pyknotic osteocytes were observed within the irregular distribution of the $OPG^{-/-}$ OLCS (Fig. 2D). In cortical bone of the wild-type mice, the endosteal region showed more regular OLCS than that seen in epiphyses, in which the longitudinal axis of osteocytes were parallel to the bone surfaces, and the osteocytes extended their cytoplasmic processes perpendicular to the surface (Fig. 2E). Most areas of the $OPG^{-/-}$ cortical bone showed a well-aligned OLCS except the periphery of invading soft tissue with an irregular OLCS (Fig. 2F). Thus, the OLCS of $OPG^{-/-}$ mice was irregular in the epiphyses, but well-arranged in the cortical bone except the region of invading soft tissue.

Immunolocalization of DMP1 and sclerostin in $OPG^{-/-}$ epiphyses and cortical bone

DMP1-positive osteocytes were evenly distributed throughout the wild-type epiphyses and cortical bone (Figs. 3A, E). At higher magnification, osteocytic canaliculi and lacunae of the wild-type animals were shown to be immunopositive for DMP1 (Fig. 3C). $OPG^{-/-}$ epiphyses revealed not only decreased DMP1-immunoreactivity, but also uneven distribution (Figs. 3B, D). Unlike epiphyses, the $OPG^{-/-}$ cortical bone showed intense DMP1 immunoreactivity in many osteocytes (Fig. 3F). Statistical analyses demonstrated a significant difference in the percentage of DMP1-positive epiphyseal osteocytes in comparison with the wild-type epiphyses (Table 1; 56.91 ± 8.24 in $OPG^{-/-}$ *vs* 85.37 ± 3.87 in wild-type, $P < 0.005$), but no significantly different index in the cortical bone (Table 1; 87.48 ± 5.09 in $OPG^{-/-}$ *vs* 86.23 ± 4.21 in wild-type, NS). Taken together, DMP1 appears to be abundantly synthesized in the regularly-arranged OLCS in the wild-type epiphyses and cortical bone, as well as in the $OPG^{-/-}$ cortical bones.

Scrolostin-immunoreactivity was seen in the osteocytes and/or their lacunae of the wild-type epiphyses. Unlike DMP1, both epiphyses and cortical bone of $OPG^{-/-}$ mice showed extremely-reduced sclerostin-immunoreactivity, compared with those of the wild-type mice (Fig. 4). Consistently, statistical analyses verified a significant reduction in the index of sclerostin-positive osteocytes in the epiphyses (Table 1; 15.21 ± 4.63 in $OPG^{-/-}$ *vs* 62.96 ± 11.59 in wild-type, $P < 0.005$) and diaphyseal cortical bones (31.55 ± 8.00 in $OPG^{-/-}$ *vs* 72.26 ± 11.90 in wild-type, $P < 0.005$), when compared with that of the wild-type specimens. Thus, even distribution of DMP1-positivity was seen in the regularly-arranged OLCS in the wild-type epiphyses and cortical bone, as well as in $OPG^{-/-}$ cortical bone. However, the immunoreactivity of sclerostin was markedly reduced in both epiphyses and cortical bone of the $OPG^{-/-}$ mice.

Triple staining for ALP, TRAP and sclerostin in the wild-type and $OPG^{-/-}$ epiphyses and cortical bone

A discrepancy in the localization of DMP1 and sclerostin prompted us to examine whether other factors than the regularity of OLCS would affect the synthesis of sclerostin. Because sclerostin was shown to be associated with osteoblastic activities and subsequent bone formation (33, 37), we examined triple staining for ALP and TRAP, hallmarks for osteoblastic and osteoclastic lineages, in addition to localizing sclerostin (Fig. 5). As a result, $OPG^{-/-}$ epiphyses and cortical bone showed a thick layer of ALP-positive osteoblasts accompanied with many TRAP-positive osteoclasts. Few sclerostin-positive osteocytes were seen close to a thick cell layer of ALP-positive and TRAP-positive cells (Figs. 5D, H). However, osteocytes apart from the bone surface, *i.e.,* those located in the inner portion of the bone matrix revealed intense sclerostin immunoreactivity. Consistently, statistical analyses showed an increased percentage in TRAP-positive areas in the $OPG^{-/-}$ epiphyses (Table1; 3.53 ± 1.17 in $OPG^{-/-}$ *vs* 1.03 ± 0.81 in wild-type, $P < 0.05$) and cortical bones (2.49 ± 0.79 in $OPG^{-/-}$ *vs* 0.67 ± 0.66 in wild-type, $P < 0.005$). The percentage of ALP-positive areas was significantly higher in the $OPG^{-/-}$ epiphyses (5.38 ± 1.69 in $OPG^{-/-}$ *vs* 1.34 ± 0.83 in wild-type, $P < 0.005$) and cortical bone (4.60 ± 1.34 in $OPG^{-/-}$ *vs* 0.78 ± 0.35 in wild-type, $P < 0.01$) when compared with that of their wild-type counterparts. Despite the presence of regular OLCS, $OPG^{-/-}$ cortical bone showed a statistically attenuated percentage in the number of sclerostin-positive osteocytes when compared with that of the wild-type specimens as described above (Table 1).

DISCUSSION

The currently accepted postulation states that osteocytes serve in the transport of small molecules, local mineralization and regulation of bone metabolism (1, 8, 14, 35). The establishment of a regular distribution of OLCS by physiological remodeling appears

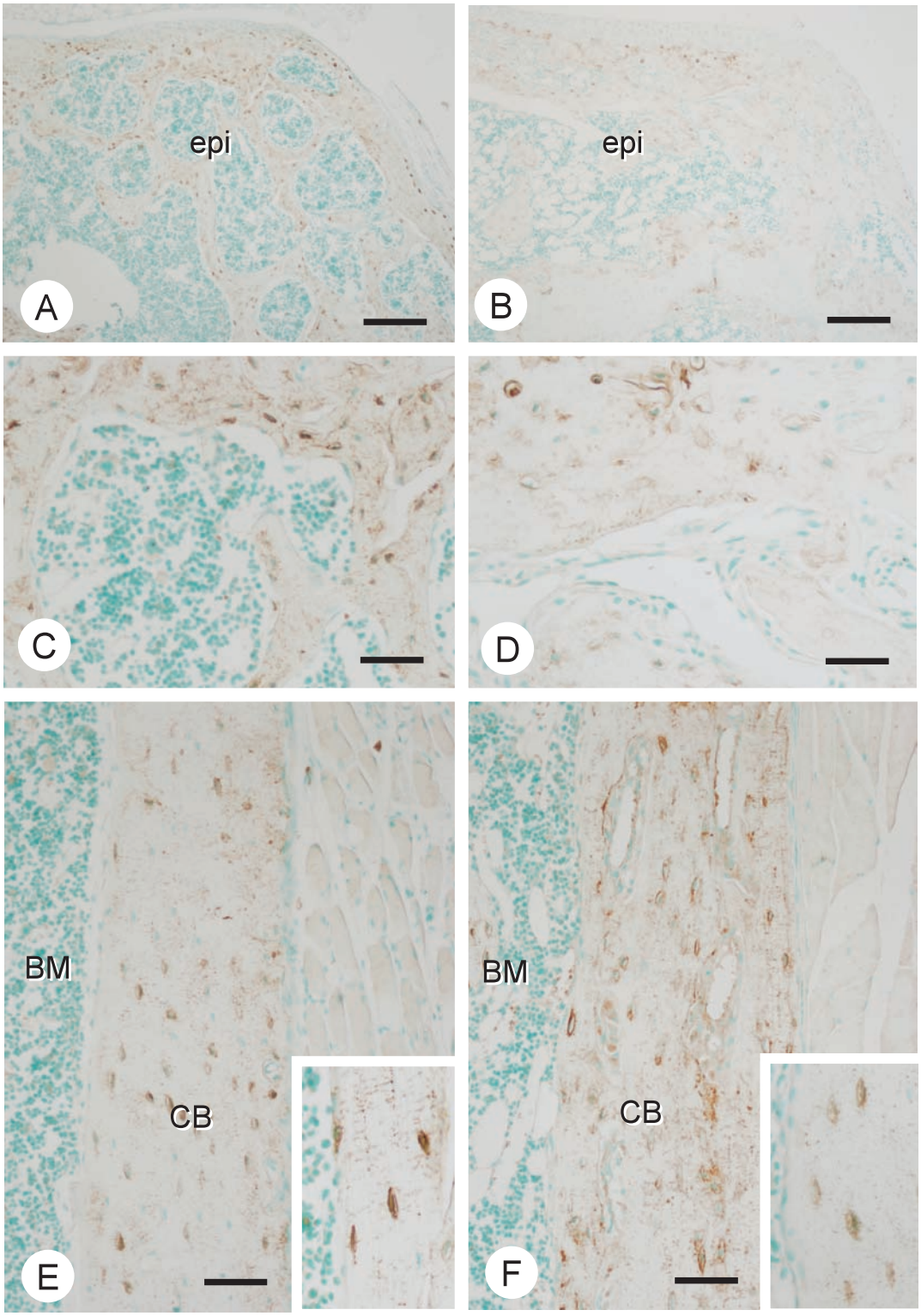

Fig. 3 Immunolocalization of DMP1 (brown) in the wild-type mice (A, C, E) and OPG$^{-/-}$ mice (B, D, F). The wild-type epiphyses (epi) showed evenly distributed DMP1-positive osteocytes (A, C). However, in the OPG$^{-/-}$ mice, the immunoreactivity of DMP1 was weaker than that seen in the wild-type counterparts (B, D). At higher magnification, OPG$^{-/-}$ epiphyses (D) revealed not only decreased immunoreactivity, but also uneven distribution of DMP1-positivity, when compared with that of the wild-type mice (C). Unlike epiphyses, the OPG$^{-/-}$ cortical bone (CB) showed intense DMP1 immunoreactivity in many osteocytes (See insets in E and F). BM: bone marrow, Bars: 200 μm (A and B), 70 μm (C and D), and 100 μm (E and F)

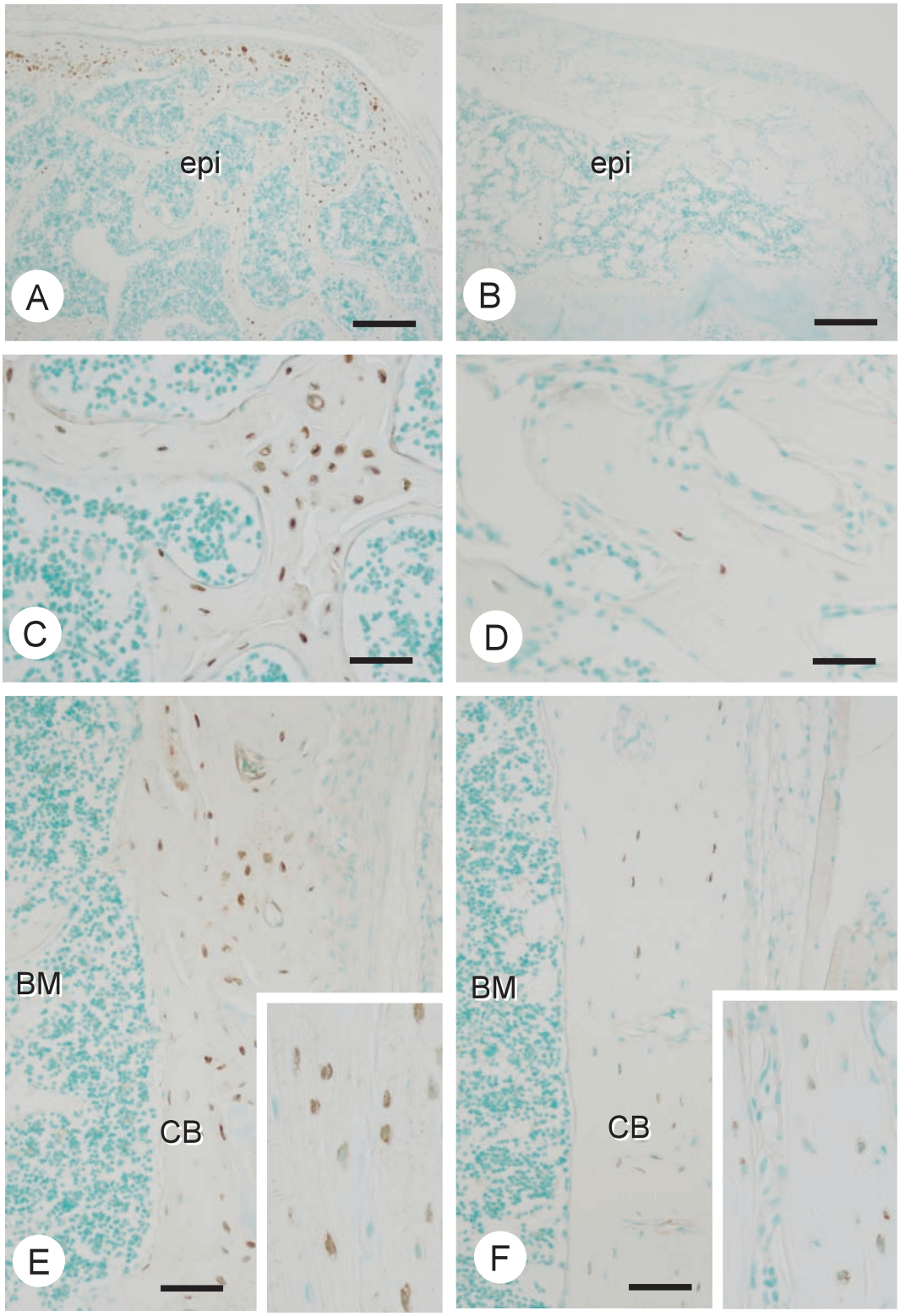

Fig. 4 Immunolocalization of sclerostin (brown) in the wild-type mice (A, C, E) and OPG$^{-/-}$ mice (B, D, F). Screlostin-immunoreactivity was seen in the osteocytes of the wild-type epiphyses (A, C) and cortical bone (E). However, both OPG$^{-/-}$ epiphyses (B, D) and cortical bone (F) revealed markedly reduced sclerostin-immunoreactivity. Note weak immunopositivity of sclerostin in OPG$^{-/-}$ osteocytes (Compare insets in E and F). epi: epiphyses, CB: cortical bone, BM: bone marrow, Bars: 200 μm (A and B), 70 μm (C and D), and 100 μm (E and F)

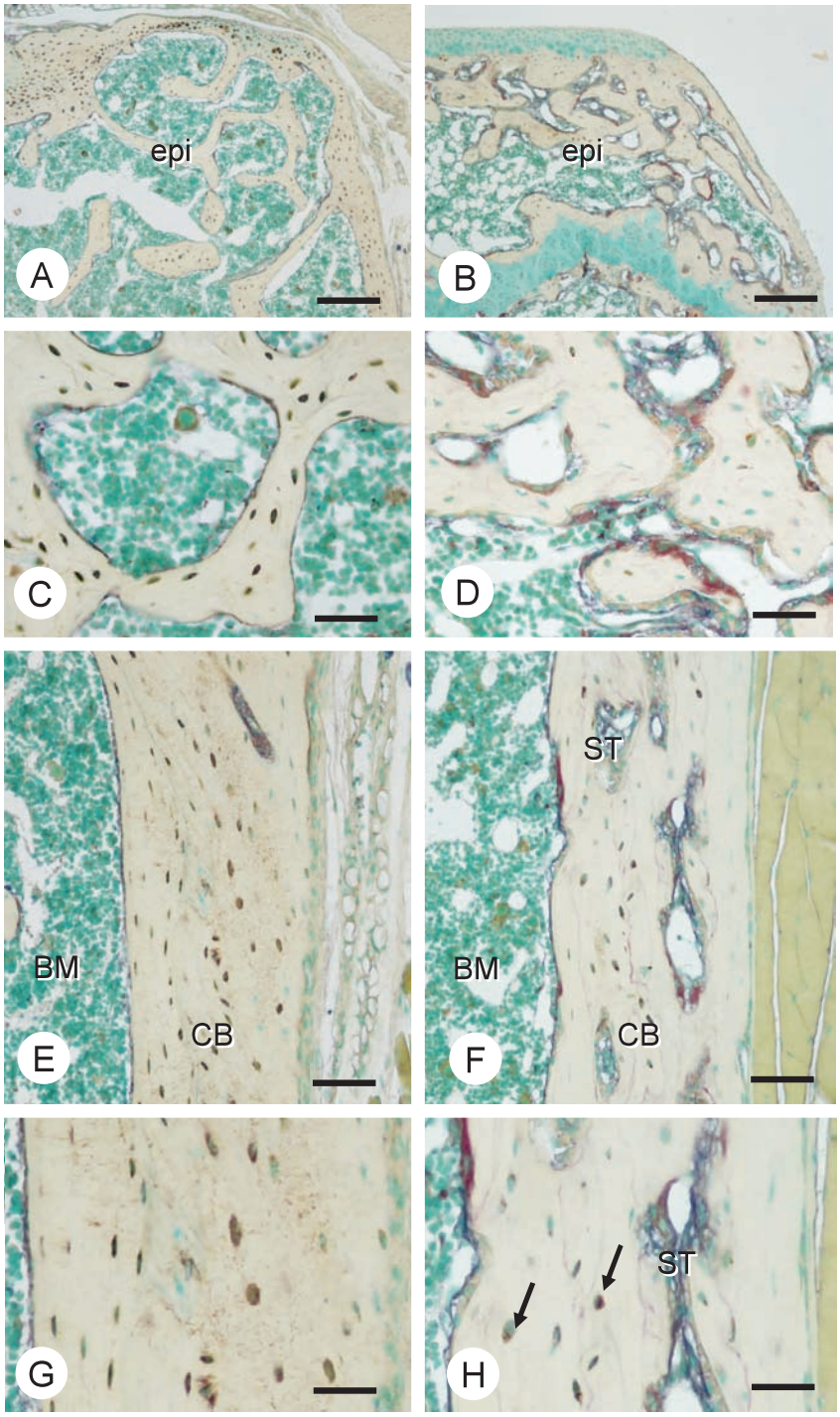

Fig. 5 Triple staining for ALP (blue), TRAP (red) and sclerostin (brown). OPG$^{-/-}$ epiphyses (epi) revealed a thick layer of ALP-positive osteoblasts accompanied with many TRAP-positive osteoclasts (B, D) compared with the wild-type ones (A, C). Many sclerostin-positive (brown) osteocytes were present in the wild-type epiphyses (C), while few sclerostin-positive osteocytes can be seen in the OPG$^{-/-}$ epiphyses (D). The endosteal surface of wild-type cortical bone (CB) was covered with ALP-positive flattened cells, and there were few TRAP-osteoclasts (E, G). However, OPG$^{-/-}$ cortical bone localized many ALP-positive osteoblastic cells (blue) and TRAP-positive osteoclasts (red) on its surface and also in the inner regions (F, H). See plump osteoblasts (blue) covering the pore in the inner region of the cortical bone. However, note that osteocytes (arrows), which are apart from the thick osteoblastic layer on the bone surface in the inner regions, reveal intense immunoreactivity for sclerostin (brown). BM: bone marrow, ST: soft tissue, Bars: 200 μm (A and B), 50 μm (C and D), 100 μm (E and F), and 50 μm (G and H)

Table 1 *Statistical analysis of the percentage of DMP1-positive or sclerostin-positive cells in the total numbers of osteocytes, as well as the percentage of ALP-positive and TRAP-positive areas*

	epiphyses		cortical bone	
	wild-type	OPG$^{-/-}$	wild-type	OPG$^{-/-}$
DMP1	85.37 ± 3.87	56.91 ± 8.24[a]	86.23 ± 4.21	87.48 ± 5.09
sclerostin	62.96 ± 11.59	15.21 ± 4.63[a]	72.26 ± 11.90	31.55 ± 8.00[a]
ALP	1.34 ± 0.83	5.38 ± 1.69[a]	0.78 ± 0.35	4.60 ± 1.34[c]
TRAP	1.03 ± 0.81	3.53 ± 1.17[b]	0.67 ± 0.66	2.49 ± 0.79[a]

The percentage of DMP1-positive or sclerostin-positive cells in the total numbers of osteocytes was determined in the epiphyseal trabecules and cortical bone of the wild-type and OPG$^{-/-}$ mice. The index of ALP-positive and TRAP-positive areas was also examined in the corresponding region of these mice. Statistical analysis was performed by the paired Student's *t*-test (See Materials and methods). All data is expressed as mean ± standard deviation. [a]$P < 0.005$, [b]$P < 0.05$, [c]$P < 0.01$

to be essential for maturation of the bone matrix (13, 31). This study provides clues for better understanding of osteocytic function in which the regular distribution of OLCS may chiefly affect DMP1 synthesis, but the cellular activities of osteoclasts and osteoblasts may ultimately influence the synthesis of sclerostin.

Assuming that the regularly-arranged OLCS is a matured, fully functional syncytium, it seems reasonable that a more abundant amount of DMP1, which is involved in mineralization, could be produced by such osteocytes. As shown in Fig. 2, silver impregnation has demonstrated the disturbed distribution of OLCS including empty lacunae in the epiphyses, but the OLCS was regularly arranged in the cortical bone of the OPG$^{-/-}$ mice. According to the degree of OLCS's regularity, DMP1-reactivity was reduced in OPG$^{-/-}$ epiphyses, but intense in cortical bone. Thus, the synthesis of DMP1 may be, at least, controlled by the geometrical regularity of OLCS. However, one may notice that these findings might be seemingly contradictable to our previous reports which demonstrated DMP1 even in the poorly-arranged OLCS in normal mice (31). As shown in Fig. 2D, there were several empty lacunae in the OPG$^{-/-}$ epiphyses, and such bone does not seem to be merely subjected to accelerated bone remodeling, but also to pathological osteocytes' death. The intercellular signaling among OLCS appears to be abruptly interrupted by the presence of empty lacunae, and might lessen the osteocytic function of OLCS. Taken together, it seems likely that the geometrical regularity of OLCS is essential for osteocytic function including DMP1 synthesis, but pathologically excessive bone remodeling would disrupt the syncytium of OLCS.

Interestingly, OPG$^{-/-}$ mice kept well-arranged distribution of OLCS, featuring an intense immunoreactivity of DMP1 in cortical bone. We postulate that, even in the circumstance of accelerated osteoclastogenesis by an OPG deficiency, the sites being easily resorbed and remodeled might be different according to each part of the long bone. For example, at seventeen weeks after birth, the epiphyseal growth plate and metaphyseal trabecules had been already enclosed in the OPG$^{-/-}$ mice, due to stimulated bone resorption (Fig. 1B). This indicates that metaphysis is the site always being subjected to osteoclastic bone resorption, and might be easily collapsed by pathologically-enhanced bone resorption. In contrast, both the epiphyses and diaphyseal cortical bone are the sites bearing the mechanical load —body weight and physical practices. Especially, cortical bone may be the most important part to retain bone structure against stimulated bone resorption and mechanical loading. In our study, OPG$^{-/-}$ cortical bone showed porosity, but was not totally fragmented, keeping the trunk of the femora. For the above-mentioned reason, cortical bone may not be completely resorbed, resulting in a well-organized arrangement of OLCS even under an OPG deficiency.

We wondered why sclerostin but not DMP1 showed less immunoreactivity in the OPG$^{-/-}$ cortical bone in spite of the regular distribution of OLCS. Osteocytes close to a thick layer of ALP-positive osteoblasts and TRAP-positive osteoclasts showed little sclerostin immunoreactivity, while osteocytes apart from the bone surface tended to show abundant sclerostin molecules (Fig. 5). Therefore, it seems possible that cellular activities of osteoblasts, rather than the regularity of OLCS, might eventually influence sclerostin synthesis.

Our next question was how could sclerostin synthesis be reduced in OPG$^{-/-}$ cortical bone? Since osteocytes are not targets for OPG, we assumed that

osteocytes might recognize the cellular activities of osteoclasts and osteoblasts in the OPG$^{-/-}$ framework, prior to synthesizing sclerostin. Many reports have suggested that osteocytes secrete sclerostin to inhibit osteoblastic activities (18, 32, 34, 37), which implies intercellular signaling derived from osteocytes toward osteoblasts on the bone surface. However, a reverse signaling direction between osteocytes and osteoblast/osteoclasts on bone surfaces might exist, *i.e.,* a signaling from osteoblasts/osteoclasts toward osteocytes embedded in the bone matrix. The present study seems, at least, to indicate this possibility that synthesis of sclerostin might be controlled by the cellular microenvironment surrounding osteocytes, rather than the regulation of the OLCS. Further detailed experiments are necessary to verify this postulation.

Acknowledgements

This study was partially supported by grants from Japanese Society for the Promotion of Science (Amizuka N, Li M, Suzuki R).

REFERENCES

1. Aarden EM, Burger EH and Nijweide PJ (1994) Function of osteocytes in bone. *J Cell Biochem* **55**, 287–299.
2. Amizuka N, Takahashi N, Udagawa N, Suda T and Ozawa H (1997) An ultrastructural study of cell-cell contact between mouse spleen cells and calvaria-derived osteoblastic cells in a co-culture system for psteoclast formation. *Acta Histochem Cytochem* **30**, 351–362.
3. Amizuka N, Shimomura J, Li M, Seki Y, Oda K, Henderson JE, Mizuno A, Ozawa H and Maeda T (2003) Defective bone remodelling in osteoprotegerin-deficient mice. *J Electron Microsc* **52**, 503–513.
4. Bélanger LF (1969) Osteocytic osteolysis. *Calcif Tissue Res* **4**, 1–12.
5. Bodian D (1936) A new method for staining nerve fibers and nerve endings in mounted paraffin section. *Anat Rec* **65**, 89–97.
6. Bodian D (1937) The staining of paraffin sections of nerve tissue with activated protagol. The role of fixatives. *Anat Rec* **69**, 153–162.
7. Burger EH and Klein-Nulend J (1999) Mechanotransduction in bone role of the lacuno-canalicular network. *FASEB J* **13**, 101–112.
8. Burger EH (1995) Sensitivity of osteocytes to biomechanical stress in vitro. *FASEB J* **9**, 441–445.
9. Doty SB (1981) Morphological evidence of gap junctions between bone cells. *Calcif Tissue Int* **33**, 509–512.
10. Feng JQ, Ward LM, Liu S, Lu Y, Xie Y, Yuan B, Yu X, Rauch F, Davis SI, Zhang S, Rios H, Drezner MK, Quarles LD, Bonewald LF and White KE (2006) Loss of DMP1 causes rickets and osteomalacia and identifies a role for osteocytes in mineral metabolism. *Nat Genet* **38**, 1230–1231.
11. Freitas de Luis HP, Li M, Ninomiya T, Nakamura M, Ubaidus S, Oda K, Udagawa N, Maeda T, Takagi R and Amizuka N (2009) Intermittent PTH administration stimulates pre-osteoblastic proliferation without leading to enhanced bone formation in osteoclast-less c-fos(-/-) mice. *J Bone Miner Res* **24**, 1586–1597.
12. George A, Gui J, Jenkins NA, Gilbert DJ, Copeland NG and Veis A (1994) *In situ* localization and chromosomal mapping of the AG1 (Dmp1) gene. *J Histochem Cytochem* **42**, 1527–1531.
13. Hirose S, Li M, Kojima T, de Freitas PH, Ubaidus S, Oda K, Saito C and Amizuka N (2007) A histological assessment on the distribution of the osteocytic lacunar canalicular system using silver staining. *J Bone Miner Metab* **25**, 374–382.
14. Klein-Nulend J, van der Plas A, Semeins CM, Ajubi NE, Frangos JA, Nijweide PJ and Burger EH (1995) Sensitivity of osteocytes to biomechanical stress in vitro. *FASEB J* **9**, 441–445.
15. Knothe Tate ML, Adamson JR, Tami AE and Bauer TW (2004) The osteocyte. *Int J Biochem Cell Biol* **36**, 1–8.
16. Kusu N, Laurikkala J, Imanishi M, Usui H, Konishi M, Miyake A, Thesleff I and Itoh N (2003) Sclerostin is a novel secreted osteoclast-derived bone morphogenetic protein antagonist with unique ligand specificity. *J Biol Chem* **278**, 24113–24117;
17. Lacey DL, Timms E, Tan HL, Kelley MJ, Dunstan CR, Burgess T, Elliott R, Colombero A, Elliott G, Scully S, Hsu H, Sullivan J, Hawkins N, Davy E, Capparelli C, Eli A, Qian YX, Kaufman S, Sarosi I, Shalhoub V, Senaldi G, Guo J, Delaney J and Boyle WJ (1998) Osteoprotegerin ligand is a cytokine that regulates osteoclast differentiation and activation. *Cell* **93**, 165–176.
18. Li X, Zhang Y, Kang H, Liu W, Liu P, Zhang J, Harris SE and Wu D (2005) Sclerostin binds to LRP5/6 and antagonizes canonical Wnt signaling. *J Biol Chem* **280**, 19883–19887.
19. Li X, Ominsky MS, Warmington KS, Morony S, Gong J, Cao J, Gao Y, Shalhoub V, Tipton B, Haldankar R, Chen Q, Winters A, Boone T, Geng Z, Niu QT, Ke HZ, Kostenuik PJ, Simonet WS, Lacey DL and Paszty C (2009) Sclerostin antibody treatment increases bone formation, bone mass, and bone strength in a rat model of postmenopausal osteoprosis. *J Bone Miner Res* **24**, 578–588.
20. Lin C, Jiang X, Dai Z, Guo X, Weng T, Wang J, Li Y, Feng G, Gao X and He L (2009) Sclerostin mediates bone response to mechanical unloading via antagonizing Wnt/betacatenin signaling. *J Bone Miner Res* **24**, 1641–1661.
21. Oda K, Amaya Y, Fukushi-Irie M, Kinameri Y, Ohsuye K, Kubota I, Fujimura S and Kobayashi J (1999) A general method for rapid purification of soluble versions of glycosylphosphatidylinositol-anchored proteins expressed in insect cells: an application for human tissue-nonspecific alkaline phosphatase. *J Biochem* **126**, 694–699.
22. Poole KE, van Bezooijen RL, Loveridge N, Hamersma H, Papapoulos SE, Löwik CW and Reeve J (2005) Sclerostin is a delayed secreted product of osteocytes that inhibits bone formation. *FASEB J* **19**, 1842–1844.
23. Shapiro F (1997) Variable conformation of GAP junctions linking bone cells: a transmission electron microscopic study of linear stacked linear, curvilinear, oval, and annular junctions. *Calcif Tissue Int* **61**, 285–293.
24. Silvestrini G, Ballanti P, Leopizzi M, Sebastiani M, Berni S, Di Vito M and Bonucci E (2007) Effects of intermittent parathyroid hormone (PTH) administration on SOST mRNA and protein in rat bone. *J Mol Histol* **38**, 261–269.
25. Simonet WS, Lacey DL, Dunstan CR, Kelley M, Chang MS, Luthy R, Nguyen HQ, Wooden S, Bennett L, Boone T,

Shimamoto G, DeRose M, Elliott R, Colombero A, Tan HL, Trail G, Sullivan J, Davy E, Bucay N, Renshaw-Gegg L, Hughes TM, Hill D, Pattison W, Campbell P, Sander S, Van G, Tarpley J, Derby P, Lee R and Boyle WJ (1997) Osteoprotegerin: a novel secreted protein involved in the regulation of bone density. *Cell* **89**, 309–319.

26. Suda T, Takahashi N, Udagawa N, Jimi E, Gillespie MT and Martin TJ (1999) Modulation of osteoclast differentiation and function by the new members of the tumor necrosis factor receptor and ligand families. *Endocrine Rev* **20**, 345–357.
27. Tatsumi S, Ishii K, Amizuka N, Li M, Kobayashi T, Kohno K, Ito M, Takeshita S and Ikeda K (2007) Targeted ablation of osteocytes induces osteoporosis with defective mechanotransduction. *Cell Metab* **5**, 464–475.
28. Takahashi N, Udagawa N, Akatsu T, Tanaka H, Isogai Y and Suda T (1991) Deficiency of osteoclasts in osteopetrotic mice is due to a defect in the local microenvironment provided by osteoblastic cells. *Endocrinology* **128**, 1792–1796.
29. Toyosawa S, Shintani S, Fujiwara T, Ooshima T, Sato A, Ijuhin N and Komori T (2001) Dentin matrix protein 1 is predominantly expressed in chicken and rat osteocytes but not in osteoblasts. *J Bone Miner Res* **16**, 2017–2026.
30. Tsukii K, Shima N, Mochizuki S, Yamaguchi K, Kinosaki M, Yano K, Shibata O, Udagawa N, Yasuda H, Suda T and Higashio K (1998) Osteoclast differentiation factor mediates an essential signal for bone resorption induced by 1 alpha,25-dihydroxyvitamin D3, prostaglandin E2, or parathyroid hormone in the microenvironment of bone. *Biochem Biophys Res Commun* **246**, 337–341.
31. Ubaidus S, Li M, Sultana S, de Freitas PH, Oda K, Maeda T, Takagi R and Amizuka N (2009) FGF23 is mainly synthesized by osteocytes in the regularly distributed osteocytic lacunar canalicular system established after physiological bone remodeling. *J Electron Microsc* **58**, 381–392.
32. van Bezooijen RL, Roelen BA, Visser A, van der Wee-Pals L, de Wilt E, Karperien M, Hamersma H, Papapoulos SE, ten Dijke P and Löwik CW (2004) Sclerostin is an osteocyte-expressed negative regulator of bone formation, but not a classical BMP antagonist. *J Exp Med* **199**, 805–814.
33. van Bezooijen RL, ten Dijke P, Papapoulos SE and Löwik CW (2005) SOST/sclerostin, an osteocyte-derived negative regulator of bone formation. *Cytokine Growth Factor Rev* **16**, 319–327.
34. Veverka V, Henry AJ, Slocombe PM, Ventom A, Mulloy B, Muskett FW, Muzylak M, Greenslade K, Moore A, Zhang L, Gong J, Qian X, Paszty C, Taylor RJ, Robinson MK and Carr MD (2009) Characterization of the structural features and interactions of sclerostin: molecular insight into a key regulator of Wnt-mediated bone formation. *J Biol Chem* **284**, 10890–10900.
35. Weinbaum S, Cowin SC and Zeng Y (1994) A model for the excitation of osteocytes by mechanical loading-induced bone fluid shear stresses. *J Biomech* **27**, 339–360.
36. Whyte MP, Obrecht SE, Finnegan PM, Jones JL, Podgornik MN, McAlister WH and Mumm S (2002) Osteoprotegerin deficiency and juvenile Paget's disease. *N Engl J Med* **347**, 175–184.
37. Winkler DG, Sutherland MK, Geoghegan JC, Yu C, Hayes T, Skonier JE, Shpektor D, Jonas M, Kovacevich BR, Staehling-Hampton K, Appleby M, Brunkow ME and Latham JA (2003) Osteocyte control of bone formation via sclerostin, a novel BMP antagonist. *EMBO J* **22**, 6267–6276.
38. Yasuda H, Shima N, Nakagawa N, Yamaguchi K, Kinosaki M, Mochizuki S, Tomoyasu A, Yano K, Goto M, Murakami A, Tsuda E, Morinaga T, Higashio K, Udagawa N, Takahashi N and Suda T (1998) Osteoclast differentiation factor is a ligand for osteoprotegerin/osteoclastogenesis-inhibitory factor and is identical to TRANCE/RANKL. *Proc Natl Acad Sci USA* **95**, 3597–3602.